

# Drastic magnetic-field-induced chiral current order and emergent current-bond-field interplay in kagome metal $AV_3Sb_5$ (A=Cs,Rb,K)

Rina Tazai<sup>1\*</sup>, Youichi Yamakawa<sup>2\*</sup>, and Hiroshi Kontani<sup>2</sup>

<sup>1</sup>*Yukawa Institute for Theoretical Physics, Kyoto University, Kyoto 606-8502, Japan*

<sup>2</sup>*Department of Physics, Nagoya University, Nagoya 464-8602, Japan*

(Dated: March 2, 2023)

In kagome metals, the chiral current order  $\boldsymbol{\eta}$  with time-reversal-symmetry-breaking is the source of various exotic electronic states, while the method of controlling the current order and its interplay with the star-of-David bond order  $\boldsymbol{\phi}$  are still unsolved. Here, we reveal that tiny uniform orbital magnetization  $M_{\text{ch}}[\boldsymbol{\eta}, \boldsymbol{\phi}]$  is induced by the chiral current order, and its magnitude is prominently enlarged under the presence of the bond order. Importantly, we derive the magnetic-field ( $h_z$ )-induced Ginzburg-Landau free energy expression  $\Delta F[h_z, \boldsymbol{\eta}, \boldsymbol{\phi}]$ , which enables us to elucidate the field-induced current-bond phase transitions in kagome metals. The emergent current-bond- $h_z$  trilinear coupling term in the free-energy,  $-3m_1 h_z \boldsymbol{\eta} \cdot \boldsymbol{\phi}$ , naturally explains the characteristic magnetic field sensitive electronic states in kagome metals, such as the field-induced current order and the strong interplay between the bond and current orders.

## Introduction

Recent discovery of unconventional quantum phases in metals has led to a new trend of condensed matter physics. Exotic charge-density-wave orders and unconventional superconductivity in geometrically frustrated kagome metal  $AV_3Sb_5$  (A=Cs,Rb,K) have been attracting increasing attention [1, 2]. The  $2 \times 2$  (inverse) star-of-David order, which is presumably the triple- $\mathbf{q}$  ( $3Q$ ) bond order (BO), occurs at  $T_{\text{BO}} \approx 100$  K at ambient pressure [3, 4]. The BO is the time-reversal-symmetry (TRS) preserving modulation in the hopping integral,  $\delta t_{ij}^{\text{b}} = \text{real}$ . [5–10]. Below  $T_{\text{BO}}$ , nodeless superconductivity occurs for A=Cs [11, 12], which is naturally explained based on the BO fluctuation mechanism proposed in Ref. [10].

In kagome metals, unusual TRS breaking (TRSB) phase without long-range spin orders has been reported by  $\mu$ -SR [13–16], Kerr rotation [17, 18], field-tuned chiral transport [19] measurements and STM studies under magnetic field [3, 19]. The transition temperature  $T_{\text{TRSB}}$  is still under debate. Although it is close to  $T_{\text{BO}}$  in many experiments, the TRSB order parameter is strongly magnified at  $T^* \approx 35$ K for A=Cs [13, 15, 19] and  $T^* \approx 50$ K for A=Rb [16]. Recently, magnetic torque measurement reveals the nematic order with TRSB at  $T^{**} \approx 130$ K [20], while no TRSB was reported by recent Kerr rotation study [21]. A natural candidate is the correlation driven TRSB hopping integral modulation:  $\delta t_{ij}^{\text{c}} = \text{imaginary}$ . This order accompanies topological charge-current [22] that gives the giant anomalous Hall effect (AHE) [23, 24]. Theoretically, the current order is mediated by strong BO fluctuations, which is naturally expected from the phase diagram of kagome metals [25].

The cascade of rich quantum phases in kagome met-

als gives rise to various exotic electronic states. A notable example is the emergent nematic ( $C_2$ ) order inside the BO and the current-order phases, which is observed by the elastoresistance, [26] the scanning birefringence [17], and the STM [4] studies. Thus, exotic electronic states can be realized inside the current-BO coexisting phases [7–10, 25, 27, 28]. Sizable off-site interaction due to beyond-MFA mechanism [29–37] leads to the current order and  $C_2$  coexisting state in kagome metals [25].

In kagome metals, outer magnetic field  $h_z$  drastically modifies the electronic states. The chirality of the charge-current is aligned under very tiny  $|h_z| \sim 0.5$  Tesla according to the measurements of AHE [23, 24] and field-tuned chiral transport [19]. In addition, the amplitude of the loop current is strongly magnified by applying small  $h_z$  ( $\gtrsim 1$  Tesla) [14–16]. These drastic  $h_z$ -dependences are the hallmarks of the TRSB state, and it is urgent to understand the coupling between the current order, chirality and the magnetic field in kagome metals.

In this paper, we reveal that the  $3Q$  loop-current order parameters accompany tiny orbital magnetization,  $M_{\text{ch}}$ , and its magnitude is drastically enlarged under the presence of the bond order. Importantly, we derive the  $h_z$ -induced Ginzburg-Landau (GL) free energy expression  $\Delta F$ , which is useful to reveal the electronic states under  $h_z$  in future. The emergent current-bond- $h_z$  trilinear coupling term in  $\Delta F$  not only explains the origin of novel field-induced chiral symmetry breaking [14–16] but also provides useful hints to control the charge current in kagome metals.

## Model Hamiltonian with current and bond orders

Here, we study the kagome-lattice tight-binding model with  $b_{3g}$ -orbitals shown in Fig. 1 (a). Each unit-cell is composed of three sublattices A, B, C. We set the nearest-neighbor hopping integral  $t = -0.5$ [eV]. In ad-

\*These authors made equal contribution to the work.

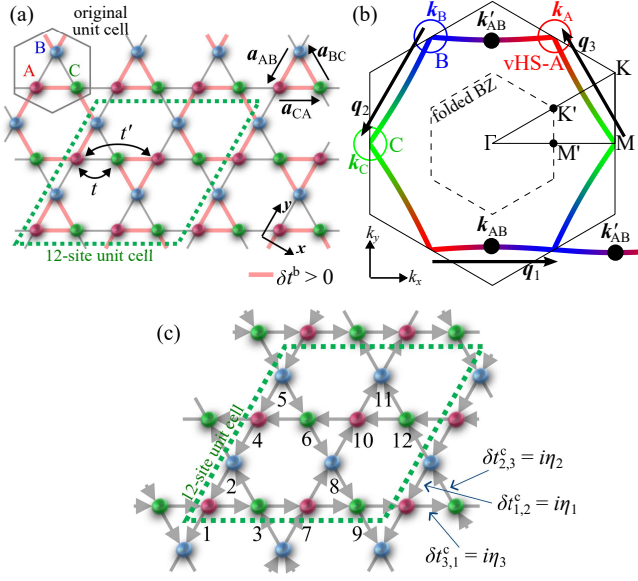


FIG. 1: (a) Kagome lattice tight-binding model. The  $3Q$  BO  $\phi = (\phi, \phi, \phi)/\sqrt{3}$  ( $\phi > 0$ ) is depicted. (b) FS at the vHS filling  $n_{\text{vHS}}$ . Three vHS points  $\mathbf{k}_A$ ,  $\mathbf{k}_B$  and  $\mathbf{k}_C$  are respectively composed of A (red), B (blue), and C (green) orbitals. The inter-vHS nesting vectors  $\mathbf{q}_n$  ( $n = 1, 2, 3$ ) are shown. (c)  $3Q$  current order  $\boldsymbol{\eta} = (\eta_1, \eta_2, \eta_3)$  is depicted. Note that  $(\eta_1, \eta_2, \eta_3)$  and  $(\eta_1, -\eta_2, -\eta_3)$  are the same bulk states.

dition, we introduce the nearest intra-sublattice hopping  $t' = -0.02[\text{eV}]$  shown in Fig. 1 (a) to avoid the perfect nesting. (Hereafter, the unit of the energy is eV.) The Fermi surface (FS) at the van-Hove singularity (vHS) filling,  $n = n_{\text{vHS}} = 2.55$  per 3-site unit cell, is shown in Fig. 1 (b). Then, the FS lies on the three vHS points ( $\mathbf{k}_A$ ,  $\mathbf{k}_B$ ,  $\mathbf{k}_C$ ), each of which is composed of a single sublattice A, B, or C. This simple three-orbital model well captures the main pure-type FS in kagome metals [3, 38–40].

The bond/current order is the modulation of the hopping integral between  $i$  and  $j$  atoms,  $\delta t_{ij}^{b/c}$ , which is the symmetry breaking in the self-energy that is derived from the density-wave (DW) equation [10, 25]. The wavevectors of the bond and current orders correspond to the inter-sublattice nesting vectors  $\mathbf{q}_n$  ( $n = 1, 2, 3$ ) in Fig. 1 (b) according to previous theoretical studies [7–10, 25, 27]. The triple  $Q$  ( $3Q$ ) current order between the nearest atoms is depicted in Fig. 1 (c). The form factor (=normalized order parameter) with  $\mathbf{q} = \mathbf{q}_1$ ,  $f_{ij}^{(1)}$ , is  $+i$  for  $(i, j)$  belongs to the sites  $(l, m) = (1, 2), (2, 4), (4, 5), (5, 1)$  in Fig. 1 (c), and  $-i$  for  $(i, j)$  belongs to  $(7, 8), (8, 10), (10, 11), (11, 7)$ . Odd parity relation  $f_{ij}^{(1)} = -f_{ji}^{(1)}$  holds. Other form factors with  $\mathbf{q}_2$  and  $\mathbf{q}_3$ ,  $f_{ij}^{(2)}$  and  $f_{ij}^{(3)}$ , are also derived from Fig. 1 (c). Using  $\mathbf{f}_{ij} = (f_{ij}^{(1)}, f_{ij}^{(2)}, f_{ij}^{(3)})$ , the current order is

$$\delta t_{ij}^c = \boldsymbol{\eta} \cdot \mathbf{f}_{ij}, \quad (1)$$

where  $\boldsymbol{\eta} \equiv (\eta_1, \eta_2, \eta_3)$  is the set of current order param-

eters with the wavevector  $\mathbf{q}_m$ . Also, the BO is given as

$$\delta t_{ij}^b = \boldsymbol{\phi} \cdot \mathbf{g}_{ij}, \quad (2)$$

where  $\boldsymbol{\phi} \equiv (\phi_1, \phi_2, \phi_3)$  is the set of BO parameters with the wavevector  $\mathbf{q}_m$ , and  $g_{ij}^{(m)} = g_{ji}^{(m)} = \pm 1$  is the even-parity form factor for the BO shown in Fig. 1 (a). (For example,  $g_{i,j}^{(1)} = +1$  [ $-1$ ] for  $(i, j)$  belongs to  $(1, 2), (4, 5), (8, 10), (11, 7)$  [ $(2, 4), (5, 1), (7, 8), (10, 11)$ ].)

The unit cell under the  $3Q$  bond/current order is magnified by  $2 \times 2$  times. Thus, we analyze the electronic states with the current order based on the 12-site kagome lattice model. The Hamiltonian with the current+bond order is  $\hat{H} = \sum_{\mathbf{k}, l, m, \sigma} h_{lm}(\mathbf{k}) c_{\mathbf{k}, l, \sigma}^\dagger c_{\mathbf{k}, m, \sigma}$ , where  $l, m = 1 \sim 12$  and  $h_{lm}(\mathbf{k}) (= h_{ml}(\mathbf{k})^*)$  is the Fourier transform of the nearest-neighbor hopping integral  $\tilde{t}_{ij} = t_{ij} + \delta t_{ij}^b + \delta t_{ij}^c$ . Here,  $t_{ij}$  is the hopping integral of the original model, and  $\delta t_{ij}^{b(c)}$  is the hopping integral due to the bond (current) order in Eq. (2) (Eq. (1)).

### Uniform orbital magnetization

The TRS is broken in the presence of the current order  $\delta t_{ij}^c$ . In this case, the orbital magnetization  $M_{\text{ch}}$  may appear due to the finite Berry curvature.  $M_{\text{ch}}$  per V atom in the unit of Bohr magneton  $\mu_B = e\hbar/2m_e c$  ( $m_e =$  free electron mass) is given as [9, 41, 42]

$$M_{\text{ch}} = \frac{\mu_B}{E_0 N_{\text{uc}} N} \sum_{\mathbf{k}, \sigma, \alpha \neq \beta} \text{Im}(\mathbf{V}_{\beta\alpha\mathbf{k}}^* \times \mathbf{V}_{\beta\alpha\mathbf{k}})_z \times \left( (\epsilon_{\beta\mathbf{k}} - \epsilon_{\alpha\mathbf{k}}) n(\epsilon_{\alpha\mathbf{k}}) - 2T \ln[1 + e^{-(\epsilon_{\alpha\mathbf{k}} - \mu)/T}] \right), \quad (3)$$

$$\mathbf{V}_{\alpha\beta\mathbf{k}} = \langle \alpha\mathbf{k} | \nabla_{\mathbf{k}} h_{\mathbf{k}} | \beta\mathbf{k} \rangle / (\epsilon_{\alpha\mathbf{k}} - \epsilon_{\beta\mathbf{k}}), \quad (4)$$

where  $\epsilon_{\alpha\mathbf{k}}$  is  $\alpha$ -th eigenenergy of  $\hat{h}_{\mathbf{k}}$  in the unit of eV,  $n(\epsilon)$  is Fermi distribution function,  $N_{\text{uc}} = 12$  is the site number of  $2 \times 2$  unit cell,  $N$  is the  $\mathbf{k}$ -mesh number, and  $E_0 = \hbar^2/a^2 m_e$ .  $a$  is the unit length in the numerical study, and we set  $a = |\mathbf{a}_{AB}| (= 0.275 \text{ nm}$  in kagome metals).  $E_0 = 0.5$  [0.28] eV when  $a = 0.4$  [0.3] nm.

At zero temperature, Eq. (3) is rewritten as  $M_{\text{ch}} = \frac{\mu_B}{E_0 N_{\text{uc}} N} \sum_{\mathbf{k}, \alpha < \beta} \text{Im}\{V_{\beta\alpha\mathbf{k}}^x V_{\beta\alpha\mathbf{k}}^y - (\alpha \leftrightarrow \beta)\} (\epsilon_{\alpha\mathbf{k}} + \epsilon_{\beta\mathbf{k}} - 2\mu)(n(\epsilon_{\alpha\mathbf{k}}) - n(\epsilon_{\beta\mathbf{k}}))$ . Considering the factor  $(n(\epsilon_{\alpha\mathbf{k}}) - n(\epsilon_{\beta\mathbf{k}}))$  with  $\alpha < \beta$ ,  $M_{\text{ch}}$  originates from the virtual particle-hole excitation between  $|\alpha\mathbf{k}\rangle$  ( $\epsilon_{\alpha\mathbf{k}} < \mu$ ) and  $|\beta\mathbf{k}\rangle$  ( $\epsilon_{\beta\mathbf{k}} > \mu$ ). All vHS points A, B, C in Fig. 1 (b) move to  $\Gamma$  point in the folded Brillouin zone (BZ), and they are hybridized by the current form factor. When  $n \approx n_{\text{vHS}}$ , the hybridization occurs near the Fermi level, so the bonding (antibonding) band energy at  $\Gamma$  point is below (above) the Fermi level. Because  $|\text{Im}\{\dots\}| \propto |\epsilon_{\alpha\mathbf{k}} - \epsilon_{\beta\mathbf{k}}|^{-2}$ ,  $M_{\text{ch}}$  becomes large when  $n \approx n_{\text{vHS}}$ .

Here, we calculate  $M_{\text{ch}}$  [ $\mu_B$ ] near the vHS filling  $n_{\text{vHS}} = 2.55$  at  $T = 1 \text{ meV}$ , in the case of  $E_0 = 0.5 \text{ eV}$ . Figure 2 (a) represents the obtained  $M_{\text{ch}}$  under the  $3Q$  current order

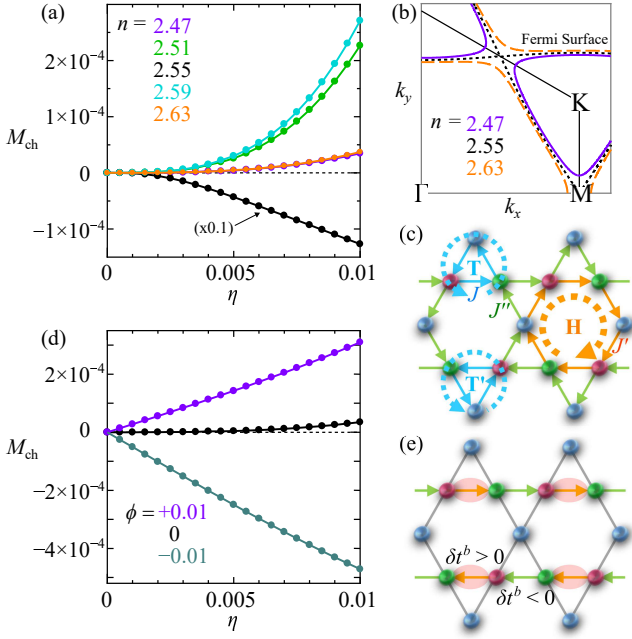


FIG. 2: (a)  $M_{\text{ch}}$  [ $\mu_{\text{B}}$ ] per V atom due to the 3Q current order  $\boldsymbol{\eta} = (\eta, \eta, \eta)/\sqrt{3}$  at  $T = 1\text{meV}$  for  $n = 2.47 \sim 2.63$ .  $M_{\text{ch}} (\propto \eta^3)$  is large when  $n \approx n_{\text{vHS}}$ . (b) FS around  $n_{\text{vHS}} = 2.55$ . (c) Charge-current pattern in real space.  $J \neq J' \neq J''$  in spite of the same order parameter  $\eta_1 = \eta_2 = \eta_3$ . (d)  $M_{\text{ch}} (\propto \eta)$  due to the coexistence of 3Q current order and 3Q BO at  $n = 2.47$ . (e) 1Q bond+current order with finite  $M_{\text{ch}}$ . Its time-reversal and translation by  $2\mathbf{a}_{\text{AB}}$  causes a different state.

$\boldsymbol{\eta} = (\eta, \eta, \eta)/\sqrt{3}$  for  $n = 2.47 \sim 2.63$ . (The FS without the current order is shown in Fig. 2 (b).) We obtain the relation  $M_{\text{ch}} \propto \eta^3$ , and it becomes large when the filling is close to  $n_{\text{vHS}}$ . Therefore, the 3Q current order state is a weak-ferromagnetic (or ferrimagnetic) state. Because the additional free energy under the magnetic field  $h_z$  per 3-site unit cell is

$$\Delta F = -3h_z M_{\text{ch}}, \quad (5)$$

the chirality of the current order is aligned under tiny  $h_z$ . In other words, the 3Q current order is stabilized under  $h_z$ . In contrast,  $M_{\text{ch}} = 0$  for 1Q and 2Q current orders.  $h_z = 10^{-4}$  corresponds to  $\sim 1$  Tesla.

Here, we present a symmetry argument to understand  $M_{\text{ch}}$  induced by the current order. Both 1Q and 2Q current orders are invariant under the time-reversal and the translational operations successively. Therefore,  $M_{\text{ch}} = 0$  due to the TRS in the bulk state. In contrast,  $M_{\text{ch}}$  is nonzero in the 3Q current order because this state breaks the TRS in the bulk state [9]. To find an intuitive reason, we calculated the charge-current along the nearest bonds  $J_{ij}$  in the 3Q state using the method in Refs. [36, 43], and found that  $|J_{ij}|$  is bond-dependent in spite of the same order parameter  $\eta_1 = \eta_2 = \eta_3$ . The obtained relation  $J \neq J' \neq J''$  shown in Fig. 2 (c) indicates that

$M_{\text{ch}}$  becomes finite because the magnetic fluxes through triangles and hexagons do not cancel perfectly.

For general order parameter  $\boldsymbol{\eta} = (\eta_1, \eta_2, \eta_3)$ , we verified the relation  $M_{\text{ch}} \propto \eta_1 \eta_2 \eta_3$  up to the third-order. In fact, based on the perturbation theory with respect to Eq. (1);  $\eta_m \hat{f}^{(m)}$  ( $m = 1 - 3$ ).  $M_{\text{ch}}[\boldsymbol{\eta}]$  is expanded as  $\sum b_{pqr} \eta_1^p \eta_2^q \eta_3^r$  with  $p + q + r = \text{odd}$  because  $M_{\text{ch}}[\boldsymbol{\eta}]$  is an odd function of  $\boldsymbol{\eta}$ . In addition,  $b_{pqr}$  can be nonzero only when  $p\mathbf{q}_1 + q\mathbf{q}_2 + r\mathbf{q}_3 = \mathbf{0}$  (in the original unfolded BZ) because we consider the uniform magnetization. In Fig. 2 (a),  $M_{\text{ch}}$  originates from the third-order term  $b_{111}$ , which is allowed because of the momentum conservation  $\mathbf{q}_1 + \mathbf{q}_2 + \mathbf{q}_3 = \mathbf{0}$ .

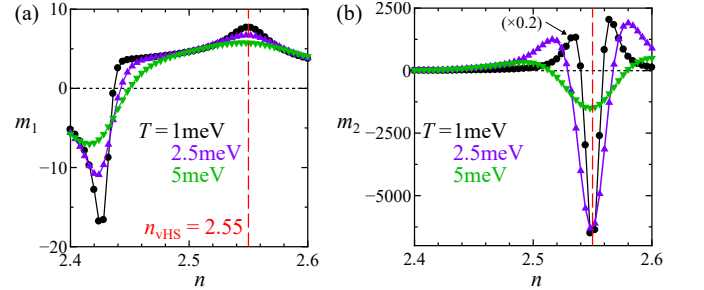


FIG. 3: Obtained coefficients of  $\bar{M}_{\text{ch}}$ , (a)  $m_1$  and (b)  $m_2 (= -m_3)$ , per V atom as a function of  $n$ . Both  $|m_1|$  and  $|m_2|$  are large for  $n \sim n_{\text{vHS}}$ , and  $m_1$  changes its sign when  $\mathbf{k}_{\text{AB}}$  and  $\mathbf{k}'_{\text{AB}}$  in the original BZ (in Fig.1 (b)) touch in the folded BZ.

Next stage, we calculate  $M_{\text{ch}}$  under the coexistence of the 3Q current order  $\boldsymbol{\eta} = (\eta, \eta, \eta)/\sqrt{3}$  and the 3Q bond order  $\boldsymbol{\phi} = (\phi, \phi, \phi)/\sqrt{3}$ . Figure 2 (d) represents  $M_{\text{ch}}$  at  $\phi = 0, \pm 0.01$  as a function of  $\eta$ , for  $n = 2.47$  and  $T = 1\text{meV}$ . Interesting relation  $M_{\text{ch}} \propto \eta$  is obtained when  $\phi \neq 0$ . Then, the field-induced  $\Delta F$  contains a non-analytic  $\eta$ -linear term that always produces  $\langle \eta \rangle \neq 0$ . This fact causes significant field-induced change in the phase diagram, as we will discuss later (see SM D [44]).

To understand the  $\eta$ -linear term in Fig. 2 (d), we expand  $M_{\text{ch}}$  with respect to the current order  $\eta_m \hat{f}^{(m)}$  and bond order  $\phi_m \hat{g}^{(m)}$ . Its Taylor expansion is  $\sum b'_{prq} \eta_1^p \eta_2^q \eta_3^r \phi_1^{p'} \phi_2^{q'} \phi_3^{r'}$  with  $p + q + r = \text{odd}$  and  $(p + p')\mathbf{q}_1 + (q + q')\mathbf{q}_2 + (r + r')\mathbf{q}_3 = \mathbf{0}$  (in the unfolded BZ). The  $\eta$ -linear term in Fig. 2 (c) mainly originates from the second-order term  $b'_{100}$  in addition to the third-order term  $b'_{100}$ . In fact, the 1Q current + 1Q BO state shown in Fig. 2 (e) violates the TRS in the bulk state.

### Field-induced GL free energy expression

From the above discussions, we obtain the following convenient expression of the orbital magnetization and the “field-induced GL free energy formula” up to the third-order:

$$\bar{M}_{\text{ch}} = m_1 \boldsymbol{\phi} \cdot \boldsymbol{\eta} + m_2 \eta_1 \eta_2 \eta_3$$

$$+m_3(\eta_1\phi_2\phi_3 + \phi_1\eta_2\phi_3 + \phi_1\phi_2\eta_3), \quad (6)$$

$$\Delta\bar{F} = -3h_z\bar{M}_{\text{ch}}, \quad (7)$$

which enables us to elucidate the field-induced current-bond phase transitions in kagome metals. Figure 3 shows the coefficients  $m_1$  and  $m_2$  derived from Eq. (3) numerically. Interestingly,  $|m_1|$  and  $|m_2|$  become large for  $n \sim n_{\text{vHS}}$ . In addition,  $m_1$  changes its sign at  $n = 2.44$ , at which  $\mathbf{k}_{\text{AB}}$  and  $\mathbf{k}'_{\text{AB}}$  in the original BZ (in Fig.1 (b)) touch in the folded BZ. Therefore, both  $|m_1|$  and  $|m_2|$  are large for a wide range of  $n$ , so the field-induced  $\Delta\bar{F}$  should be significant in real kagome metals.

In SM A [44], we show that  $\bar{M}_{\text{ch}}$  in Eq. (6) well reproduces the original  $M_{\text{ch}}$  when  $|\eta|, |\phi| \lesssim 0.02$ . We verified in SM B [44] that the magnitudes of  $m_1$  and  $m_2$  at  $t' = -0.08$  is comparable to those in Fig. 3. Here, we obtain  $m_3 = -m_2$  because a simple relation  $f_{ij}^{(m)} = ig_{ij}^{(m)}$  or  $-ig_{ij}^{(m)}$  is satisfied when both order parameters are composed of only the nearest bonds. However, these order parameters possess different long-range components in the microscopic mechanism [25], so the relation  $m_3 = -m_2$  is not exact.

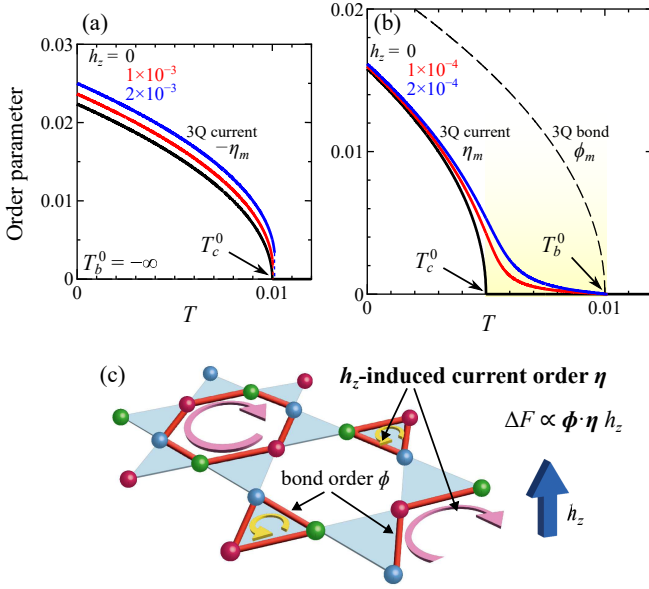


FIG. 4: Obtained  $\eta_m$  ( $m = 1, 2, 3$ ) for  $d_4/2d_3 = 0.5$  under  $h_z$ .  $h_z = 10^{-4}$  corresponds to 1 Tesla. (a) 3Q current order with  $T_c^0 = 0.01$  and  $T_b^0 = \infty$ . The first-order transition is induced by  $h_z$  due to  $m_2$ -term. (b) 3Q current order with  $T_c^0 = 0.005$  under the 3Q BO with  $T_b^0 = 0.01$ . For  $h_z \neq 0$ ,  $\eta$  starts to increase below  $T_b^0$  thanks to  $m_1$ -term, *i.e.*,  $T_c = T_b^0$ . (c)  $h_z$ -induced chiral current order in the shaded area in (b).

Below, we derive the order parameters under  $h_z$  by minimizing the GL free energy  $F = F^0 + \Delta\bar{F}$ , where  $F^0 = F_\eta^0 + F_\phi^0 + F_{\eta,\phi}^0$  is the free energy at  $h_z = 0$  [9, 25]:

$$F_\phi^0 = a_b|\phi|^2 + b_1\phi_1\phi_2\phi_3 + d_1(\phi_1^4 + \phi_2^4 + \phi_3^4) + d_2(\phi_1^2\phi_2^2 + (\text{cycl.})), \quad (8)$$

$$F_\eta^0 = a_c|\boldsymbol{\eta}|^2 + d_3(\eta_1^4 + \eta_2^4 + \eta_3^4) + d_4(\eta_1^2\eta_2^2 + (\text{cycl.})), \quad (9)$$

and  $F_{\eta,\phi}^0$  is the current-bond cross term that is proportional to  $\eta^2\phi^b$  with  $b = 1, 2$ . Here,  $a_{c(b)} = r_{c(b)}(T - T_{c(b)}^0)$ , where  $T_{c(b)}^0$  is the current-order (BO) transition temperature without other orders. Theoretically,  $a_{c(b)} \sim N(0)(-1 + \lambda_{\eta(\phi)}^{-1})$ , where  $N(0)$  is the density-of-states ( $\sim 1\text{eV}^{-1}$ ) and  $\lambda_{\eta(\phi)}$  is the DW equation eigenvalue of the current order (bond order) [45].  $\lambda_{\eta(\phi)} = 1$  at  $T = T_{c(b)}^0$ , while  $\lambda_{\eta(\phi)} = 0$  (*i.e.*,  $a_{c(b)} = \infty$ ) in the absence of interaction. According to Ref. [45],  $r_b T_b^0 \sim 0.1N(0)$  for the nematic BO in FeSe, while the corresponding value for BCS superconductors is  $\sim N(0)$ .

To discuss the phase diagram qualitatively, we set  $m_1 = 5$ ,  $m_2 = -m_3 = -1000$ , both of which are moderate compared with the values in Fig. 3. We also put  $d_i = 150$  ( $i = 1-4$ ) by seeing the numerical results in SM C [44] and set  $r_c = r_b = 30$ . To concentrate on the field-induced novel phenomena, *i.e.*, the field-induced chirality and non-analytic free energy, we drop  $F_{\eta,\phi}^0$  and  $b_1$ -term. Then, both current and bond orders become 3Q states because of the relations  $2d_1/d_2 > 1$  and  $2d_3/d_4 > 1$ . A more detailed explanation for the GL parameters is presented in the SM C [44].

## Numerical results

Figure 4 (a) shows the obtained 3Q current order  $\boldsymbol{\eta} = (\eta_1, \eta_2, \eta_3)$  with  $\eta_1 = \eta_2 = \eta_3$ , when  $T_c^0 = 0.01$  in the absence of BO ( $T_b^0 = -\infty$ ). Here, we set  $h_z = 0 \sim 2 \times 10^{-3}$ . Because of the  $\eta^3$ -term by  $m_2 = -1000$ , 3Q current order  $\boldsymbol{\eta} = (\eta, \eta, \eta)/\sqrt{3}$  with negative  $\eta$  is stabilized in the presence of  $h_z > 0$ . In addition, the field-induced first-order transition occurs at  $T = T_c^0 + \Delta T_c$ , where  $\Delta T_c = (h_z m_2)^2 / 4r_c(d_3 + d_4)$  is quite small.

Figure 4 (b) exhibits the 3Q current order with  $T_c^0 = 0.005$ , in the presence of the BO with  $T_b^0 = 0.01$ . For  $h_z = 1 \times 10^{-4}$  and  $2 \times 10^{-4}$ ,  $\eta$  starts to increase just below  $T_b^0$  thanks to the  $\eta$ -linear term  $\Delta\bar{F} = -3h_z(m_1\phi + m_3\phi^2)\eta$ , and therefore  $T_c = T_b^0$ . When  $h_z \neq 0$ ,  $T_c^0$  is just a crossover temperature. To understand the role of the non-analytic term qualitatively, we analyze a simple GL free energy with a  $\eta$ -linear term in SM D [44]: It is found that the field-induced current order  $|\boldsymbol{\eta}_{\text{ind}}|$  under the BO  $\phi$  is approximately given as

$$|\boldsymbol{\eta}_{\text{ind}}| \approx 9|m_1 h_z \phi| / 2a_c. \quad (10)$$

Thus, the field-induced  $|\boldsymbol{\eta}_{\text{ind}}|$  is prominent when the system at  $h_z = 0$  is close to the current order state (*i.e.*,  $a_c \gtrsim 0$ ) The expression of  $|\boldsymbol{\eta}_{\text{ind}}|$  in Eq. (10) is proportional to  $\phi$  in contrast to Eq. (31) of Ref. [9]. A schematic picture for the field-induced current order is shown in Fig. 4 (c).

In the BO phase with  $\boldsymbol{\phi} = (\phi, \phi, \phi)$ , the field-induced  $\boldsymbol{\eta}$  above  $T_c^0$  is proportional to  $\boldsymbol{\phi}$  to maximize  $|\bar{M}_{\text{ch}}|$ , so this

coexisting state has  $C_6$  symmetry [25]. It is noteworthy that the coexisting state at  $h_z = 0$  has  $C_2$  symmetry due to the third-order term of  $F_{\eta,\phi}^0$ ; see Ref. [25].) When  $f_{ij}^{(m)} = \pm i g_{ij}^{(m)}$ , the current order is suppressed by  $F_{\eta,\phi}^0$  when  $T_c^0 < T_b^0$  and  $r_c = r_b$  [9]. However, this suppression is reduced when realistic form factors with long-range components are considered [25]. Thus, current order is realized inside the BO phase even at  $h_z = 0$ .

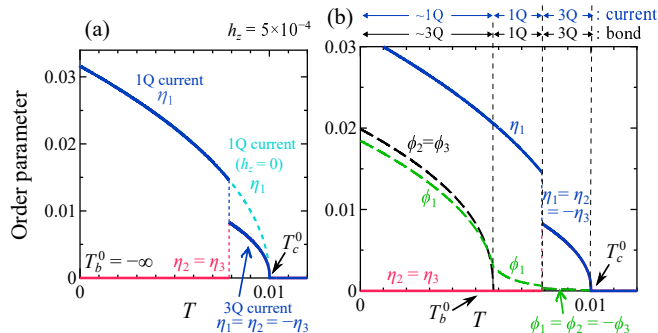


FIG. 5: Obtained  $\eta_m$  and  $\phi_m$  ( $m = 1, 2, 3$ ) for  $d_4/2d_3 = 1.2$  at  $T_c^0 = 0.01$  and  $h_z = 5 \times 10^{-4}$ , for (a)  $T_b^0 = -\infty$  and (b)  $T_b^0 = 0.005$ . In (a), 3Q order appears due to the  $m_2$ -term, while it changes to 1Q order at  $T \approx 0.008$ . In (b), field-induced BO starts to appear above  $T_b^0$  due to the  $m_1$ -term, and  $T_b^0$  is just a crossover temperature.

Next, we study the case when 1Q current order is realized at  $h_z = 0$ , by increasing  $d_4 = 150$  to 360 (*i.e.*,  $d_4/2d_3 = 1.2$ ) in the previous GL parameters. A strong evidence of the 1Q current order has been reported recently in Ref. [20]. We set  $T_c^0 = 0.01$ . Figure 5 (a) shows the obtained order parameters without BO ( $T_{BO}^0 = -\infty$ ) at  $h_z = 5 \times 10^{-4}$ . We obtain the field-induced 3Q-current order due to the  $m_2$ -term, while it changes to 1Q order at  $T \approx 0.008$ . Figure 5 (b) shows the obtained order parameters for  $T_b^0 = 0.005$ . At  $h_z = 5 \times 10^{-4}$ , the nematicity due to the 1Q BO is enlarged by  $h_z$  just below  $T_c^0$  owing to the trilinear term, and its magnitude increases with  $h_z$ . (Note that 3Q BO appears even at  $h_z = 0$  if the 3rd order term in  $F_{\eta,\phi}^0$  is not negligible.) Under  $T_b^0$ , the BO gradually changes to approximate 3Q state with  $\phi_1 \approx \phi_2 = \phi_3$ . (Here, we neglected small feedback from  $\phi$  (secondary order) to  $\eta$  (primary order).) Thus, interesting first-order transitions and the  $C_2$  phase reported in Ref. [20] would originate from the 1Q current order at  $T^{**}$  ( $> T_b^0$ ) together with  $\Delta\bar{F}$ .

In the SM E [44], we studied the case of the intra-original-unit-cell current order ( $\mathbf{q} = \mathbf{0}$ ) in kagome lattice. In this case,  $M_{ch}$  is  $\eta$ -linear even if the BO is absent.

### Summary

In summary, the chiral current order in kagome metal exhibits weak ferromagnetism, and its magnitude are en-

larged in the bond order state. Importantly, we derived the  $h_z$ -induced GL free energy expression  $\Delta\bar{F}$  in Eq. (7), which provides an important basis for future research in kagome metals. The emergent  $\eta \cdot \phi \cdot h_z$  trilinear term in  $\Delta\bar{F}$  explains prominent field-induced chiral symmetry breaking in kagome metals. This finding also provides a useful hint to control the charge current because the coefficients  $m_1$  and  $m_2$  in Fig. 3 sensitively depend on the model parameters. The analysis of the current order state with the three-dimensional layered structure is an important future issue.

We are grateful to Y. Matsuda, T. Shibauchi, K. Hashimoto, T. Asaba, S. Onari, A. Ogawa and K. Shimura for fruitful discussions. This study has been supported by Grants-in-Aid for Scientific Research from MEXT of Japan (JP18H01175, JP20K03858, JP20K22328, JP22K14003), and by the Quantum Liquid Crystal No. JP19H05825 KAKENHI on Innovative Areas from JSPS of Japan.

- [1] B. R. Ortiz, L. C. Gomes, J. R. Morey, M. Winiarski, M. Bordelon, J. S. Mangum, I. W. H. Oswald, J. A. Rodriguez-Rivera, J. R. Neilson, S. D. Wilson, E. Ertekin, T. M. McQueen, and E. S. Toberer, *New kagome prototype materials: discovery of KV<sub>3</sub>Sb<sub>5</sub>, RbV<sub>3</sub>Sb<sub>5</sub>, and CsV<sub>3</sub>Sb<sub>5</sub>*, Phys. Rev. Materials **3**, 094407 (2019).
- [2] B. R. Ortiz, S. M. L. Teicher, Y. Hu, J. L. Zuo, P. M. Sarte, E. C. Schueller, A. M. M. Abeykoon, M. J. Krogstad, S. Rosenkranz, R. Osborn, R. Seshadri, L. Balents, J. He, and S. D. Wilson, *CsV<sub>3</sub>Sb<sub>5</sub>: A Z<sub>2</sub> Topological Kagome Metal with a Superconducting Ground State*, Phys. Rev. Lett. **125**, 247002 (2020).
- [3] Y.-X. Jiang, J.-X. Yin, M. M. Denner, N. Shumiya, B. R. Ortiz, G. Xu, Z. Guguchia, J. He, M. S. Hossain, X. Liu, J. Ruff, L. Kautzsch, S. S. Zhang, G. Chang, I. Belopolski, Q. Zhang, T. A. Cochran, D. Multer, M. Litskevich, Z.-J. Cheng, X. P. Yang, Z. Wang, R. Thomale, T. Neupert, S. D. Wilson, and M. Z. Hasan, *Unconventional chiral charge order in kagome superconductor KV<sub>3</sub>Sb<sub>5</sub>*, Nat. Mater. **20**, 1353–1357 (2021).
- [4] H. Li, H. Zhao, B. R. Ortiz, T. Park, M. Ye, L. Balents, Z. Wang, S. D. Wilson, and I. Zeljkovic, *Rotation symmetry breaking in the normal state of a kagome superconductor KV<sub>3</sub>Sb<sub>5</sub>*, Nat. Phys. **18**, 265–270 (2022).
- [5] M. L. Kiesel, C. Platt, and R. Thomale, *Unconventional Fermi Surface Instabilities in the Kagome Hubbard Model*, Phys. Rev. Lett. **110**, 126405 (2013).
- [6] W.-S. Wang, Z.-Z. Li, Y.-Y. Xiang, and Q.-H. Wang, *Competing electronic orders on kagome lattices at van Hove filling*, Phys. Rev. B **87**, 115135 (2013).
- [7] X. Wu, T. Schwemmer, T. Müller, A. Consiglio, G. Sangiovanni, D. Di Sante, Y. Iqbal, W. Hanke, A. P. Schnyder, M. M. Denner, M. H. Fischer, T. Neupert, and R. Thomale, *Nature of Unconventional Pairing in the Kagome Superconductors AV<sub>3</sub>Sb<sub>5</sub> (A = K, Rb, Cs)*, Phys. Rev. Lett. **127**, 177001 (2021).
- [8] M. M. Denner, R. Thomale, and T. Neupert, *Analysis of Charge Order in the Kagome Metal AV<sub>3</sub>Sb<sub>5</sub> (A =*

- K, Rb, Cs), Phys. Rev. Lett. **127**, 217601 (2021).
- [9] T. Park, M. Ye, and L. Balents, *Electronic instabilities of kagome metals: Saddle points and Landau theory*, Phys. Rev. B **104**, 035142 (2021).
- [10] R. Tazai, Y. Yamakawa, S. Onari, and H. Kontani, *Mechanism of exotic density-wave and beyond-Migdal unconventional superconductivity in kagome metal  $AV_3Sb_5$  ( $A = K, Rb, Cs$ )*, Sci. Adv. **8**, eabl4108 (2022).
- [11] M. Roppongi, K. Ishihara, Y. Tanaka, K. Ogawa, K. Okada, S. Liu, K. Mukasa, Y. Mizukami, Y. Uwatoko, R. Grasset, M. Konczykowski, B. R. Ortiz, S. D. Wilson, K. Hashimoto, and T. Shibauchi, *Bulk evidence of anisotropic s-wave pairing with no sign change in the kagome superconductor  $CsV_3Sb_5$* , arXiv:2206.02580 (available at <https://arxiv.org/abs/2206.02580>).
- [12] W. Zhang, X. Liu, L. Wang, C. W. Tsang, Z. Wang, S. T. Lam, W. Wang, J. Xie, X. Zhou, Y. Zhao, S. Wang, J. Tallon, K. T. Lai, and S. K. Goh, *Nodeless superconductivity in kagome metal  $CsV_3Sb_5$  with and without time reversal symmetry breaking*, arXiv:2301.07374 (available at <https://arxiv.org/abs/2301.07374>).
- [13] L. Yu, C. Wang, Y. Zhang, M. Sander, S. Ni, Z. Lu, S. Ma, Z. Wang, Z. Zhao, H. Chen, K. Jiang, Y. Zhang, H. Yang, F. Zhou, X. Dong, S. L. Johnson, M. J. Graf, J. Hu, H.-J. Gao, and Z. Zhao, *Evidence of a hidden flux phase in the topological kagome metal  $CsV_3Sb_5$* , arXiv:2107.10714 (available at <https://arxiv.org/abs/2107.10714>).
- [14] C. Mielke, D. Das, J.-X. Yin, H. Liu, R. Gupta, Y.-X. Jiang, M. Medarde, X. Wu, H. C. Lei, J. Chang, P. Dai, Q. Si, H. Miao, R. Thomale, T. Neupert, Y. Shi, R. Khasanov, M. Z. Hasan, H. Luetkens, and Z. Guguchia, *Time-reversal symmetry-breaking charge order in a kagome superconductor*, Nature **602**, 245–250 (2022).
- [15] R. Khasanov, D. Das, R. Gupta, C. Mielke, M. Elender, Q. Yin, Z. Tu, C. Gong, H. Lei, E. T. Ritz, R. M. Fernandes, T. Birol, Z. Guguchia, and H. Luetkens, *Time-reversal symmetry broken by charge order in  $CsV_3Sb_5$* , Phys. Rev. Research **4**, 023244 (2022).
- [16] Z. Guguchia, C. Mielke, D. Das, R. Gupta, J.-X. Yin, H. Liu, Q. Yin, M. H. Christensen, Z. Tu, C. Gong, N. Shumiya, M. S. Hossain, T. Gamsakhurdashvili, M. Elender, P. Dai, A. Amato, Y. Shi, H. C. Lei, R. M. Fernandes, M. Z. Hasan, H. Luetkens, and R. Khasanov, *Tunable unconventional kagome superconductivity in charge ordered  $RbV_3Sb_5$  and  $KV_3Sb_5$* , Nat. Commun. **14**, 153 (2023).
- [17] Y. Xu, Z. Ni, Y. Liu, B. R. Ortiz, Q. Deng, S. D. Wilson, B. Yan, L. Balents, and L. Wu, *Three-state nematicity and magneto-optical Kerr effect in the charge density waves in kagome superconductors*, Nat. Phys. **18**, 1470–1475 (2022).
- [18] Y. Hu, S. Yamane, G. Mattoni, K. Yada, K. Obata, Y. Li, Y. Yao, Z. Wang, J. Wang, C. Farhang, J. Xia, Y. Maeno, and S. Yonezawa, *Time-reversal symmetry breaking in charge density wave of  $CsV_3Sb_5$  detected by polar Kerr effect*, arXiv:2208.08036 (available at <https://arxiv.org/abs/2208.08036>).
- [19] C. Guo, C. Putzke, S. Konyzheva, X. Huang, M. Gutierrez-Amigo, I. Errea, D. Chen, M. G. Vergniory, C. Felser, M. H. Fischer, T. Neupert, and P. J. W. Moll, *Switchable chiral transport in charge-ordered kagome metal  $CsV_3Sb_5$* , Nature **611**, 461–466 (2022).
- [20] T. Asaba *et al.*, unpublished.
- [21] D. R. Saykin, C. Farhang, E. D. Kountz, D. Chen, B. R. Ortiz, C. Shekhar, C. Felser, S. D. Wilson, R. Thomale, J. Xia, and A. Kapitulnik, *High Resolution Polar Kerr Effect Studies of  $CsV_3Sb_5$ : Tests for Time Reversal Symmetry Breaking Below the Charge Order Transition*, arXiv:2209.10570 (available at <https://arxiv.org/abs/2209.10570>).
- [22] F. D. M. Haldane, *Model for a Quantum Hall Effect without Landau Levels: Condensed-Matter Realization of the "Parity Anomaly"*, Phys. Rev. Lett. **61**, 2015 (1988).
- [23] S.-Y. Yang, Y. Wang, B. R. Ortiz, D. Liu, J. Gayles, E. Derunova, R. Gonzalez-Hernandez, L. Šmejkal, Y. Chen, S. S. P. Parkin, S. D. Wilson, E. S. Toberer, T. McQueen, and M. N. Ali, *Giant, unconventional anomalous Hall effect in the metallic frustrated magnet candidate,  $KV_3Sb_5$* , Sci. Adv. **6**, eabb6003 (2020).
- [24] F. H. Yu, T. Wu, Z. Y. Wang, B. Lei, W. Z. Zhuo, J. J. Ying, and X. H. Chen, *Concurrence of anomalous Hall effect and charge density wave in a superconducting topological kagome metal*, Phys. Rev. B **104**, L041103 (2021).
- [25] R. Tazai, Y. Yamakawa, and H. Kontani, *Charge-loop current order and  $Z_3$  nematicity mediated by bond-order fluctuations in kagome metal  $AV_3Sb_5$  ( $A=Cs, Rb, K$ )*, arXiv:2207.08068 (available at <https://arxiv.org/abs/2207.08068>).
- [26] L. Nie, K. Sun, W. Ma, D. Song, L. Zheng, Z. Liang, P. Wu, F. Yu, J. Li, M. Shan, D. Zhao, S. Li, B. Kang, Z. Wu, Y. Zhou, K. Liu, Z. Xiang, J. Ying, Z. Wang, T. Wu, and X. Chen, *Charge-density-wave-driven electronic nematicity in a kagome superconductor*, Nature **604**, 59–64 (2022).
- [27] S. Zhou and Z. Wang, *Chern Fermi pocket, topological pair density wave, and charge- $4e$  and charge- $6e$  superconductivity in kagomé superconductors*, Nat. Commun. **13**, 7288 (2022).
- [28] M. H. Christensen, T. Birol, B. M. Andersen, and R. M. Fernandes, *Loop currents in  $AV_3Sb_5$  kagome metals: multipolar and toroidal magnetic orders*, Phys. Rev. B **106**, 144504 (2022).
- [29] S. Onari and H. Kontani, *Self-consistent Vertex Correction Analysis for Iron-based Superconductors: Mechanism of Coulomb Interaction-Driven Orbital Fluctuations*, Phys. Rev. Lett. **109**, 137001 (2012).
- [30] Y. Yamakawa, S. Onari, and H. Kontani, *Nematicity and Magnetism in FeSe and Other Families of Fe-Based Superconductors*, Phys. Rev. X **6**, 021032 (2016).
- [31] S. Onari and H. Kontani,  *$SU(4)$  Valley + Spin Fluctuation Interference Mechanism for Nematic Order in Magic-Angle Twisted Bilayer Graphene: The Impact of Vertex Corrections*, Phys. Rev. Lett. **128**, 066401 (2022).
- [32] M. Tsuchiizu, Y. Ohno, S. Onari, and H. Kontani, *Orbital Nematic Instability in the Two-Orbital Hubbard Model: Renormalization-Group + Constrained RPA Analysis*, Phys. Rev. Lett. **111**, 057003 (2013).
- [33] M. Tsuchiizu, K. Kawaguchi, Y. Yamakawa, and H. Kontani, *Multistage electronic nematic transitions in cuprate superconductors: A functional-renormalization-group analysis*, Phys. Rev. B **97**, 165131 (2018).
- [34] A. V. Chubukov, M. Khodas, and R. M. Fernandes, *Magnetism, Superconductivity, and Spontaneous Orbital Order in Iron-Based Superconductors: Which Comes First and Why?*, Phys. Rev. X **6**, 041045 (2016).
- [35] R. M. Fernandes, P. P. Orth, and J. Schmalian, *Intertwined Vestigial Order in Quantum Materials: Nematicity and Beyond*, Annu. Rev. Condens. Matter Phys. **10**, 133 (2019).
- [36] H. Kontani, R. Tazai, Y. Yamakawa, and S. Onari,

- Unconventional density waves and superconductivities in Fe-based superconductors and other strongly correlated electron systems*, arXiv:2209.00539 (available at <https://arxiv.org/abs/2209.00539>).
- [37] J. C. S. Davis and D.-H. Lee, *Concepts relating magnetic interactions, intertwined electronic orders, and strongly correlated superconductivity*, Proc. Natl. Acad. Sci. U.S.A. **110**, 17623 (2013).
- [38] Y. Hu, X. Wu, B. R. Ortiz, S. Ju, X. Han, J. Ma, N. C. Plumb, M. Radovic, R. Thomale, S. D. Wilson, A. P. Schnyder, and M. Shi, *Rich nature of Van Hove singularities in Kagome superconductor CsV<sub>3</sub>Sb<sub>5</sub>*, Nat. Commun. **13**, 2220 (2022).
- [39] Y. Luo, S. Peng, S. M. L. Teicher, L. Huai, Y. Hu, B. R. Ortiz, Z. Wei, J. Shen, Z. Ou, B. Wang, Y. Miao, M. Guo, M. Shi, S. D. Wilson, and J.-F. He, *Distinct band reconstructions in kagome superconductor CsV<sub>3</sub>Sb<sub>5</sub>*, arXiv:2106.01248 (available at <https://arxiv.org/abs/2106.01248>).
- [40] Z. Liu, N. Zhao, Q. Yin, C. Gong, Z. Tu, M. Li, W. Song, Z. Liu, D. Shen, Y. Huang, K. Liu, H. Lei, and S. Wang, *Charge-Density-Wave-Induced Bands Renormalization and Energy Gaps in a Kagome Superconductor RbV<sub>3</sub>Sb<sub>5</sub>*, Phys. Rev. X **11**, 041010 (2021).
- [41] D. Ceresoli, T. Thonhauser, D. Vanderbilt, and R. Resta, *Orbital magnetization in crystalline solids: Multi-band insulators, Chern insulators, and metals*, Phys. Rev. B **74**, 024408 (2006).
- [42] J. Shi, G. Vignale, D. Xiao, and Q. Niu, *Quantum Theory of Orbital Magnetization and Its Generalization to Interacting Systems*, Phys. Rev. Lett. **99**, 197202 (2007).
- [43] R. Tazai, Y. Yamakawa, and H. Kontani, *Emergence of charge loop current in the geometrically frustrated Hubbard model: A functional renormalization group study*, Phys. Rev. B **103**, L161112 (2021).
- [44] Supplementary Materials.
- [45] R. Tazai, S. Matsubara, Y. Yamakawa, S. Onari, and H. Kontani, *Rigorous formalism for unconventional symmetry breaking in Fermi liquid theory and its application to nematicity in FeSe*, Phys. Rev. B **107**, 035137 (2023).

## [Supplementary Materials]

# Drastic magnetic-field-induced chiral current order and emergent current-bond-field interplay in kagome metal AV<sub>3</sub>Sb<sub>5</sub> (A=Cs,Rb,K)

Rina Tazai<sup>1\*</sup>, Youichi Yamakawa<sup>2\*</sup>, and Hiroshi Kontani<sup>2</sup>

<sup>1</sup>Yukawa Institute for Theoretical Physics, Kyoto University, Kyoto 606-8502, Japan

<sup>2</sup>Department of Physics, Nagoya University, Nagoya 464-8602, Japan

## A: Fitting of $M_{\text{ch}}$ by $\bar{M}_{\text{ch}}$

In the main text, we calculated the orbital magnetization  $M_{\text{ch}}$  in kagome metal with current order  $\boldsymbol{\eta}$  and bond-order  $\boldsymbol{\phi}$  using Eq. (3). Next, we derived its approximate expression up to the third-order of  $\boldsymbol{\eta}$  and  $\boldsymbol{\phi}$ :  $\bar{M}_{\text{ch}} = m_1 \boldsymbol{\phi} \cdot \boldsymbol{\eta} + m_2 \eta_1 \eta_2 \eta_3 + m_3 (\eta_1 \phi_2 \phi_3 + \text{cycl.})$ . We obtained the coefficients  $m_1$  and  $m_2$  by expanding  $M_{\text{ch}}$  with respect to  $\boldsymbol{\eta}$  and  $\boldsymbol{\phi}$  numerically. The expression  $\bar{M}_{\text{ch}}$  is very useful to understand the strong interplay between current and bond orders in kagome metal. By considering the field-induced free energy  $\Delta \bar{F} = -3h_z \bar{M}_{\text{ch}}$ , we understand the characteristic phase diagram of kagome metals under the magnetic field. Hereafter, the unit of energy is eV unless otherwise noted.

Here, we make the comparison between  $M_{\text{ch}}$  in Eq. (3) and  $\bar{M}_{\text{ch}}$  in Eq. (6). Figures S1 (a)-(c) show the obtained results at  $n = 2.47$  under  $\boldsymbol{\eta} = (\eta, \eta, \eta)/\sqrt{3}$  and  $\boldsymbol{\phi} = (\phi, \phi, \phi)/\sqrt{3}$  as functions of  $\eta$ , in the case of (a)  $\phi = 0$ , (b)  $\phi = +0.01$  and (b)  $\phi = -0.01$ . It is found that  $\bar{M}_{\text{ch}}$  well reproduce the original  $M_{\text{ch}}$  when  $|\boldsymbol{\eta}|, |\boldsymbol{\phi}| \lesssim 0.02$ , unless the shape of the Fermi surface is drastically changed by order parameters.

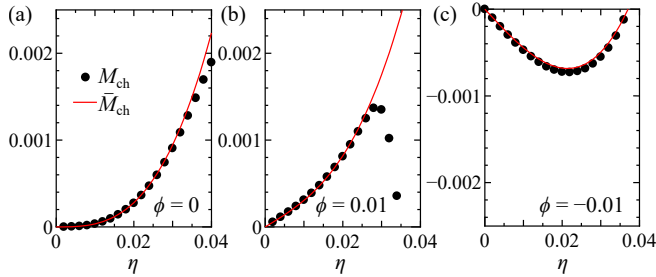


FIG. S1:  $M_{\text{ch}}$  and  $\bar{M}_{\text{ch}}$  for  $\boldsymbol{\eta} = (\eta, \eta, \eta)/\sqrt{3}$  in the cases of (a)  $\boldsymbol{\phi} = \mathbf{0}$  and (b)  $\boldsymbol{\phi} = (\phi, \phi, \phi)/\sqrt{3}$  at  $\phi = +0.01$  and (c)  $-0.01$ .

## B: $M_{\text{ch}}$ in kagome lattice model with $(t, t') = (-0.5, -0.08)$

In the main text, we studied  $M_{\text{ch}}$  in kagome lattice model with the bare hopping integrals  $(t, t') = (-0.5, -0.02)$ . The obtained coefficients  $m_1$  and  $m_2$  in  $\bar{M}_{\text{ch}}$  take large values for  $n \approx n_{\text{vHS}}$ , where  $n_{\text{vHS}}$  is the

van-Hove filling. Using the obtained coefficients  $m_1$  and  $m_2$ , we discovered the mechanism of the field-induced chiral current order in kagome metals.

To verify the robustness of the obtained results, here we analyze  $M_{\text{ch}}$  in kagome lattice model with large  $t'$ ;  $(t, t') = (-0.5, -0.08)$ . The obtained FS shown in Fig. S2 (a) has large curvature due to large  $|t'|$ . Here, we introduce the 3Q BO  $\boldsymbol{\phi} = (\phi, \phi, \phi)/\sqrt{3}$  and the 3Q current order  $\boldsymbol{\eta} = (\eta, \eta, \eta)/\sqrt{3}$ . Figure S2 (b) shows the obtained  $M_{\text{ch}}$  [ $\mu_{\text{B}}$ ] per  $V$  atom due to the 3Q current order with  $\phi = 0$ . The relation  $M_{\text{ch}} \propto \eta^3$  is satisfied, and its magnitude is enlarged when  $n \approx n_{\text{vHS}}$ . Figure S2 (c) shows  $M_{\text{ch}}$  [ $\mu_{\text{B}}$ ] due to the coexistence of 3Q current order and 3Q BO. The relation  $M_{\text{ch}} \propto \eta^1$  is satisfied when  $\phi \neq 0$ . Figures S2 (d) and (e) represent the obtained coefficients  $m_1$  and  $m_2$  in  $\bar{M}_{\text{ch}}$ . The magnitudes of  $m_1$  and  $m_2$  for  $t' = -0.08$  are comparable to those for  $t' = -0.02$  given in the main text.

## C: Calculation of GL parameters

To verify that the GL free energy coefficients assumed in the main text are qualitatively reasonable, we calculate GL coefficients based on the diagrammatic method. The 4th order GL parameters per unit cell are given as

$$d_1 = I_{1111}^g, \quad (\text{S1})$$

$$d_2 = 2I_{1212}^g + 4I_{1122}^g, \quad (\text{S2})$$

$$d_3 = I_{1111}^f, \quad (\text{S3})$$

$$d_4 = 2I_{1212}^f + 4I_{1122}^f, \quad (\text{S4})$$

where

$$\begin{aligned}
 I_{hlmn}^w &= \frac{T}{4} \sum_{k, \sigma} \text{Tr} \hat{w}_{\mathbf{q}_h}(k + \mathbf{q}_n + \mathbf{q}_m + \mathbf{q}_l) \hat{G}(k + \mathbf{q}_n + \mathbf{q}_m + \mathbf{q}_l) \\
 &\times \hat{w}_{\mathbf{q}_l}(k + \mathbf{q}_n + \mathbf{q}_m) \hat{G}(k + \mathbf{q}_n + \mathbf{q}_m) \\
 &\times \hat{w}_{\mathbf{q}_m}(k + \mathbf{q}_n) \hat{G}(k + \mathbf{q}_n) \hat{w}_{\mathbf{q}_n}(k) \hat{G}(k), \quad (\text{S5})
 \end{aligned}$$

where  $\hat{G}(k)$  is  $3 \times 3$  Green energy for the original 3-site kagome lattice model and  $k \equiv (\mathbf{k}, i\epsilon_n)$ .  $\hat{w}_{\mathbf{q}}(\mathbf{k})$  is the form factor in the momentum space,  $\hat{f}_{\mathbf{q}}(\mathbf{k})$  or  $\hat{g}_{\mathbf{q}}(\mathbf{k})$ , and  $h, l, m, n$  is 1, 2, or 3. The relation  $\mathbf{q}_h + \mathbf{q}_l + \mathbf{q}_m + \mathbf{q}_n = 0$  should be satisfied. The diagrammatic expression  $I_{hlmn}^w$



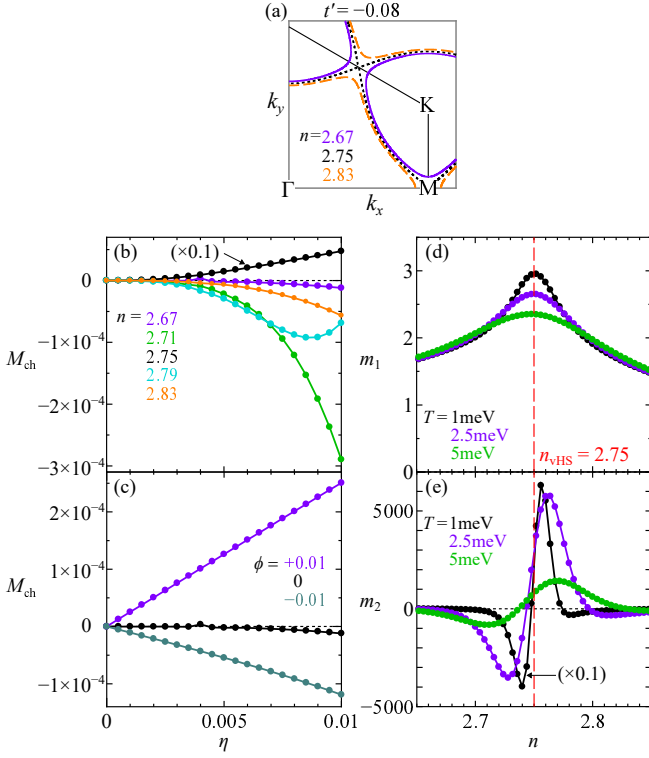


FIG. S2: (a) FS around  $n_{\text{vHS}} = 2.75$  at  $t' = -0.08$ . (b)  $M_{\text{ch}}$  [ $\mu_{\text{B}}$ ] per V atom due to the 3Q current order  $\eta = (\eta, \eta, \eta)/\sqrt{3}$  at  $T = 1\text{meV}$  for  $n = 2.67 \sim 2.83$ . (c)  $M_{\text{ch}}$  due to the coexistence of 3Q current order and 3Q BO at  $n = 2.67$ . Obtained (d)  $m_1$  and (e)  $m_2 (= -m_3)$ , per V atom as a function of  $n$ . Both  $|m_1|$  and  $|m_2|$  are large for  $n \sim n_{\text{vHS}}$ .

is depicted in Fig. S3 (a). The expressions of  $\hat{G}(k)$ ,  $\hat{f}_q(\mathbf{k})$  and  $\hat{g}_q(\mathbf{k})$  are explained in Ref. [1]. Here,  $\hat{f}_q(\mathbf{k})$  is derived microscopically in Ref. [1], and it contains distant-atom components.

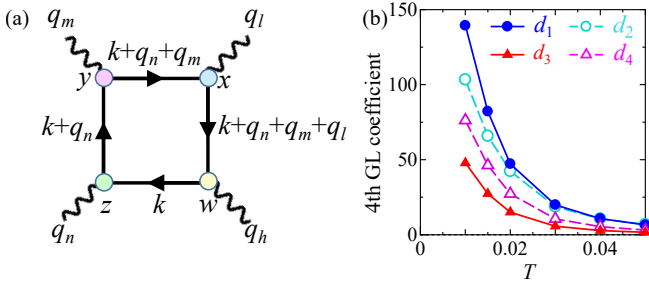


FIG. S3: (a) Diagrammatic expressions of 4th order GL parameters. (b) Numerical results of the GL parameters as functions of  $T$ .

The obtained numerical results are given in Fig. S3 (b) in the case of  $(t, t') = (-0.5, 0)$ . Here, the dimensionless form factors are normalized as  $\max_{\mathbf{k}} |g_{\mathbf{q}_1}^{\text{BA}}(\mathbf{k})| = |g_{\mathbf{q}_1}^{\text{BA}}(\mathbf{k}_A)| = 1$ . (This normalization corresponds to  $|\delta t_{ij}^b| = 1/2$ .) In the same way, we set  $\max_{\mathbf{k}} |f_{\mathbf{q}_1}^{\text{BA}}(\mathbf{k})| = |f_{\mathbf{q}_1}^{\text{BA}}(\mathbf{k}_A)| = 1$ . Thus, the parameter  $d_i = 150$  [ $\text{eV}^{-3}$ ]

is consistent with Fig. S3 (b) for  $T \sim 0.01$ . For  $\phi = (\phi, \phi, \phi)$  with  $\phi = 0.01$ , the 4th order term for the BO is  $F_4^b \sim 150 \cdot 6(10^{-2})^4 \sim 10^{-5}$  [ $\text{eV}$ ] for  $d_i = 150$ . In calculating Fig. S3 (b), we introduced the self-energy due to the BO fluctuations. The detailed explanation will be presented in the revised version of Ref. [1].

Also, the expression of the 2nd order term is derived as  $F_2^b \sim -\chi_g^0(\mathbf{q}_1)R|\phi|^2$  in Ref. [2]. Here,  $\chi_g^0(\mathbf{q}_1)$  is the irreducible BO susceptibility, and  $R \equiv (d\lambda/dT) \cdot (-T_b^0)$ , where  $\lambda$  is the eigenvalue of the density-wave equation, which is similar to the eigenvalue of the BCS gap equation.  $R \sim O(0.1)$  in usual BO phase transitions [2], while  $R \sim 1$  in BCS superconductivity because of large  $\log T$  singularity of the p-p channel. As a result,  $F_2^b \sim -3 \times 10^{-5}$  [ $\text{eV}$ ] for  $3\chi_g^0(\mathbf{q}_1) \sim 3$  and  $R = 0.1$ . Note that  $\chi_g^0(\mathbf{q}_1)R$  corresponds to  $rT_b^0 \sim 0.1$  in the main text.

Therefore, the BO total free energy is  $F_{\text{tot}}^b \sim -10^{-5}$  [ $\text{eV}$ ] for  $T_b^0 \sim \phi \sim 0.01$  and  $N(0) \sim 1$ . The current-order total free energy  $F_{\text{tot}}^c$  will be comparable to  $F_{\text{tot}}^b$ . Thus, the GL parameters assumed in the main text are qualitatively reasonable. (In BCS superconductors,  $F_{\text{tot}} = -\Delta^2 N(0)/2 \sim -10^{-4}$  when  $\Delta = 0.01$  and  $N(0) \sim 1$ .) As discussed in Ref. [2], the specific heat jump  $\Delta C/T$  at the BO or current-order phase transition is much smaller than the BCS value  $\Delta C/T_{\text{SC}} = 1.43N(0)$ .

#### D: Analysis of GL free energy with non-analytic $\eta$ -linear term

In the main text, we studied the strong interplay between the bond and current orders under the magnetic field in kagome metals. In Fig. 4, we studied the situation where bond order transition temperature  $T_b^0$  is higher than the chiral current order one  $T_c^0$  at  $h_z = 0$ . We revealed that chiral current order emerges at  $T = T_b^0$  under  $h_z \sim 10^{-4}$  ( $\sim 1\text{T}$ ). That is, the current-order transition temperature is enlarged to  $T_b^0$  under small  $h_z$ , as shown in Fig. 3 (b). The drastic field-induced 3Q current order originates from the non-analytic  $\eta$ -linear terms in  $\Delta\bar{F}$ , that is,  $\Delta\bar{F} = -3h_z[m_1\phi \cdot \eta + m_3(\eta_1\phi_2\phi_3 + \text{cycl.})] + O(\eta^3)$ .

To understand the effect of the field-induced non-analytic free energy qualitatively, we analyze the following simple GL free energy with a  $\eta$ -linear term:

$$F(\eta) = a\eta^2 + d\eta^4 - g\eta, \quad (\text{S6})$$

Here, we assume  $a$  and  $d$  are positive. When  $g \neq 0$ ,  $F(\eta)$  is minimized at finite  $\eta$  even if  $a > 0$ . The solution is given as

$$\eta_g = X^{1/3}(d^{-1} - 2 \cdot 3^{1/3}aX^{-2/3})/(2 \cdot 3^{2/3}), \quad (\text{S7})$$

$$X = 9gd^2 + \sqrt{3}\sqrt{d^3(8a^3 + 27dg^2)}. \quad (\text{S8})$$

Note that

$$\eta_g \approx g/2a \quad (\text{S9})$$

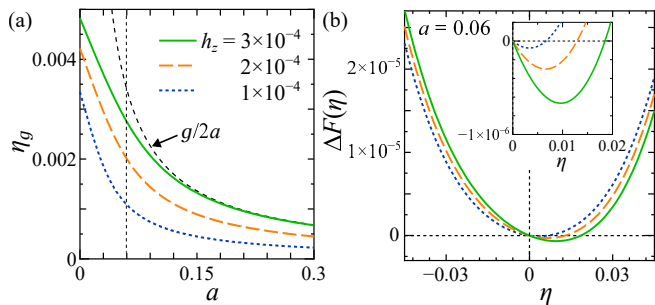


FIG. S4: (a) Induced  $\eta_g$  due to the  $\eta$ -linear term for as a function of  $a$  ( $> 0$ ). Here,  $g = 0.9h_z$  and  $h_z = 1 \sim 3 \times 10^{-4}$ . This result is not sensitive to the choice of  $d$  when  $g$  is small. (b)  $\Delta\bar{F}$  as a function of  $\eta$  for  $a = 0.06$ . (Inset) Enlarged plots around the bottoms.

for small  $g$ . Therefore,  $\eta_g$  is finite even when  $a > 0$  due to the  $\eta$ -linear term.

Here, we derive  $d$  and  $g$  from the GL free energy of kagome metal, Eqs. (9) and (8) in the main text. By setting  $\phi = (\phi, \phi, \phi)$  and  $\eta = (\eta, \eta, \eta)$  in Eqs. (9) and (8), we obtain  $d = 6d_i$  and  $g = 3(3m_1\phi + 3m_3\phi^2)h_z$ . When  $d_i = 150$ ,  $m_1 = 5$ ,  $m_3 = 1000$  and  $\phi = 0.01$ , we get  $d = 900$  and  $g = 1.35h_z$ .  $a$  in Eq. (S6) corresponds to  $3a_c$  in the main text. In Fig. 3 (b) in the main text, we set  $a_c = r_c(T - T_c^0)$  with  $r_c = 30$  and  $T_c^0 = 0.005$ , so  $T = T_c^0$  ( $2T_c^0 = T_b^0$ ) in Fig. 4 (b) corresponds to  $a = 0$  (0.45) in Eq. (S6).

Figure S4 (a) shows  $\eta_g$  given in Eq. (S8) as a function of  $a$ , in the case of  $d = 1000$  and  $g = 1.35h_z$ . We see that  $h_z \sim 10^{-4}$ , which corresponds to  $\sim 1$ T, induces sizable current order even above  $T_c^0$  if  $a \gtrsim 0$ . The obtained value of  $\eta_g$  in Fig S4 (a) at  $a \approx 0$  is comparable to the field-induced order in Fig. 4 (b). The field-induced  $\eta$  is prominent only when the system at  $h_z = 0$  is close to the current order state (*i.e.*,  $a \gtrsim 0$ ). Asymmetric  $\Delta\bar{F}$  as a function of  $\eta$  is shown in Fig S4 (b).

### E: $M_{\text{ch}}$ by intra-original-unit-cell current order in kagome lattice

Here, we calculate  $M_{\text{ch}}$  in the case of the intra-original-unit-cell ( $\mathbf{q} = \mathbf{0}$ ) current order in Fig. S2 (a). In this case,

the translational symmetry is preserved. The obtained  $M_{\text{ch}}$  is shown in Fig. S2 (b). We find that  $M_{\text{ch}}$  is  $\eta$ -linear even in the absence of the BO, while its coefficient is small for  $n \sim n_{\text{vHS}}$  that is realized in kagome metals. Regardless of the presence of the  $\eta$ -linear term in  $M_{\text{ch}}$ , field-induced intra-original-unit-cell order will be quite small in kagome metals. In fact, the field-induced cLC order at  $\mathbf{q} = \mathbf{0}$  becomes sizable only when its second-order GL coefficient,  $a_c \sim (-1 + \lambda_{\mathbf{q}=\mathbf{0}}^{-1})$ , is very small. Here,  $\lambda_{\mathbf{q}=\mathbf{0}}$  is the eigenvalue of the current order solution at  $\mathbf{q} = \mathbf{0}$ . However, the relation  $\lambda_{\mathbf{q}=\mathbf{0}} \ll 1$  is obtained in the DW equation analysis in Ref. [1].

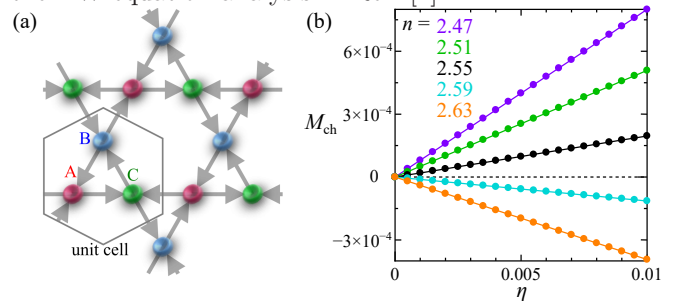


FIG. S5:  $M_{\text{ch}}$  for the intra-original-unit-cell current order  $\eta = (\eta, \eta, \eta)/\sqrt{3}$ . We set  $(t, t') = (-0.5, -0.02)$ , and no BO is introduced.

- 
- [1] R. Tazai, Y. Yamakawa, and H. Kontani, *Charge-loop current order and  $Z_3$  nematicity mediated by bond-order Fluctuations in kagome metal  $AV_3Sb_5$  ( $A = Cs, Rb, K$ )*, arXiv:2207.08068 (2022).
- [2] R. Tazai, S. Matsubara, Y. Yamakawa, S. Onari, and H. Kontani, *Rigorous formalism for unconventional symmetry breaking in Fermi liquid theory and its application to nematicity in  $FeSe$* , Phys. Rev. B **107**, 035137 (2023).